

Sept, 2020 v1.0

A Wave Optics Based Fiber Scattering Model

Supplemental document

Mandy Xia, Bruce Walter, Eric Michielssen, David Bindel, Steve Marschner

Our paper introduces the first wave optics based fiber scattering model, presenting an azimuthal fiber scattering function that comes from a full-wave simulation. Wave optics provides an alternative model that characterizes light as an electromagnetic wave that obeys Maxwell's equations, which is more accurate at all scales. Electromagnetics (EM) and Computational Electromagnetics (CEM) are the foundations of wave optics research. This supplemental document is an expanded version of the EM section (Section 4) of the main paper. However it is not possible to cover all the details and we refer the readers to classical textbooks [8, 9] and lecture notes [4] on EM, textbooks on CEM [15, 6], Optics [3] and small particle scattering [2] for more details. This supplemental document heavily relies on the above references.

This supplemental material includes a brief summary of the basic electromagnetic concepts (Section 2) we use in the paper and more detailed derivations of the solutions to the dielectric cylinder scattering problems by solving Maxwell's equations (Section 3). We describe both the numerical method using the Boundary Element Method (BEM) and the analytic solution using Lorenz-Mie theory. Finally, we explain the idea that using linearity, scattering from other kinds of illumination can be handled by first expressing them as sums of plane waves (Section 4). We use a Gaussian beam incidence field as an example as it is the incident field we use to conduct one of the validation tests.

The update-to-date version of this document can be downloaded from the [project page](#).

Contents

1	Table of symbols	3
2	Basic Electromagnetics concepts	4
2.1	Maxwell's equations	4
2.2	Plane wave	5
2.3	Poynting vector	5
3	Dielectric cylinder scattering problems	6
3.1	Problem setup	7
3.2	Boundary integrals and Boundary Element Method (BEM)	8
3.2.1	Splitting the problem via surface equivalence	8
3.2.2	Source field relations in 3D	10
3.2.3	Source field relations in 2.5D	11
3.2.4	Boundary integral equations	12
3.2.5	Boundary Element Method (BEM)	13
3.2.6	Computing far-field quantities	14
3.3	Lorenz-Mie theory	15
4	Gaussian beam	18
4.1	2.5D Gaussian beam	18
4.2	From plane wave incidence to Gaussian beam incidence	19
	References	23
A	Vector fields derivation	24

1 Table of symbols

λ	wavelength
$\theta, \theta_i, \theta_r$	polar angle, incident polar angle, outgoing polar angle
ϕ, ϕ_i, ϕ_r	azimuthal angle, incident azimuthal angle, outgoing azimuthal angle
ω_i, ω_r	incoming, outgoing direction
$S(\theta_i, \theta_r, \phi_i, \phi_o, \lambda)$	BCSDF in spherical coordinates
$M_0(\theta_i, \theta_r)$	longitudinal scattering function of mode 0
$N_p(\theta_i, \phi_i, \phi_o, \lambda)$	azimuthal scattering function of mode p
$N_{ray}, N_{wave}(\theta_i, \phi_i, \phi_o, \lambda)$	ray-based, wave-based azimuthal scattering function
$\hat{\mathbf{x}}, \hat{\mathbf{y}}, \hat{\mathbf{z}}$	unit vectors in the positive x, y, z direction.
\mathbf{r}	3D position
$\boldsymbol{\rho}, \rho$	2D position, norm of $\boldsymbol{\rho}$
Γ	boundary of cylinder cross section
\mathbf{e}_i	unit vector in the incident wave propagation direction
\mathbf{E}, \mathbf{H}	electric field, magnetic field
\mathbf{J}, \mathbf{M}	electric current, magnetic current
\mathbf{D}	electric displacement
\mathbf{B}	magnetic flux density
$\mathbf{S}, \langle \mathbf{S} \rangle$	Poynting vector, time-averaged Poynting vector
q_e, q_m	electric charge density, magnetic charge density
j	complex unit
ω	angular frequency
ϵ, μ	permittivity, permeability
\mathbf{k}	3D wave vector in ω_i direction
\mathbf{k}_ρ, k_ρ	transverse component of \mathbf{k} and its magnitude
k_z	z componnet of \mathbf{k}
G	Green's function of the Helmholtz equation.
$\mathcal{L}_i, \mathcal{K}_i, \mathcal{P}$	linear operators
$\hat{\mathbf{n}}$	normal vector
\mathbf{f}	linear basis function for currents
Z	the matrix in the boundary element method formulation
I_M, I_J	coefficients of magnetic and electric currents' basis functions
$I_s(\theta_i, \phi_i, \phi_r, \lambda)$	scattering intensity
W_s, W_a, W_x	scattering, absorption, extinction power per unit length
C_e, C_x, C_g	effective, extinction, geometric cross section
ψ	scalar wave
U	Gaussian beam in scalar form
w	Gaussian beam waist
y_c	Gaussian beam offset
N	mode number in the expansion

Table 1: We summarize the symbols used in the main paper and this document.

2 Basic Electromagnetics concepts

We will start with a brief summary of the basic concepts and equations in classical electromagnetic theory. They are the fundamentals of the methods described in later sections. A more detailed treatment on these materials can be found in [8, 9, 4].

2.1 Maxwell's equations

The mathematical description of all wave optics phenomena is based on Maxwell's equations. Fields for which the time variation is sinusoidal are called time-harmonic fields and the mathematical analysis can be simplified by using complex quantities. A complex electric field \mathbf{E} or also called a phasor is defined as related to an instantaneous electric field \mathbf{E}_{inst}

$$\mathbf{E}_{\text{inst}} = \text{Re}(\mathbf{E}e^{j\omega t}), \quad (1)$$

where ω is angular frequency. Similarly a phasor of the magnetic field \mathbf{H} is related to an instantaneous magnetic field \mathbf{H}_{inst} via

$$\mathbf{H}_{\text{inst}} = \text{Re}(\mathbf{H}e^{j\omega t}). \quad (2)$$

In what follows, we assume time-harmonic fields and time dependence $e^{j\omega t}$ is suppressed unless specified. The time-harmonic Maxwell's equations we use are [8]

$$\nabla \times \mathbf{E} = -\mathbf{M} - j\omega\mu\mathbf{H} \quad (3)$$

$$\nabla \times \mathbf{H} = \mathbf{J} + j\omega\epsilon\mathbf{E} \quad (4)$$

$$\nabla \cdot \mathbf{D} = q_e \quad (5)$$

$$\nabla \cdot \mathbf{B} = q_m. \quad (6)$$

In the above equations \mathbf{J} is the electric current density. It represents moving electric charges (e.g. electrons). In our dielectric cylinder scattering problem, they are so-called “equivalent electric current densities”, artificially introduced to create fields that satisfy appropriate boundary conditions when constructing integral equations for the fields scattered from fibers. \mathbf{D} is the electric displacement and q_e is the electric charge density. \mathbf{B} is the magnetic flux density. Magnetic current density \mathbf{M} represents moving magnetic charges and q_m is the magnetic charge density. Such charges have never been observed in nature. \mathbf{M} and q_m are entirely fictitious and introduced as mathematical auxiliary quantities solely to model fields appropriate in the construction of integral equations [8].

The cylinder scattering problem we are interested in contains linear, isotropic and non-dispersive materials for which the following constitutive relations hold.

$$\mathbf{B} = \mu\mathbf{H}, \quad \mathbf{D} = \epsilon\mathbf{E}, \quad (7)$$

where μ is the magnetic permeability and ϵ is the electric permittivity.

2.2 Plane wave

A simple solution to Maxwell's equations represents a perfectly monochromatic parallel beam of light. It is called a plane wave and it propagates in a homogeneous medium without sources. The incident electric and magnetic fields (i.e. fields in the absence of the fiber) are

$$\begin{aligned}\mathbf{E}_i(\mathbf{r}) &= \mathbf{E}_i(0) e^{j\mathbf{k}\cdot\mathbf{r}} \\ \mathbf{H}_i(\mathbf{r}) &= \mathbf{H}_i(0) e^{j\mathbf{k}\cdot\mathbf{r}} \\ \mathbf{H}_i(0) &= -\frac{\mathbf{k} \times \mathbf{E}_i(0)}{\omega\mu_0}\end{aligned}\tag{8}$$

where $\mathbf{E}_i(0)$ and $\mathbf{H}_i(0)$ define the wave's intensity and polarization, and the wavevector $\mathbf{k} = -k\mathbf{e}_i$, where \mathbf{e}_i is a real unit vector in the direction of wave propagation. The wavenumber is $k = \frac{2\pi}{\lambda}$ for light of wavelength λ and angular frequency $\omega = 2\pi/(\lambda\sqrt{\epsilon_0\mu_0})$.

2.3 Poynting vector

In electromagnetics, the *Poynting vector* represents energy flow. It can be derived from the conservation of energy, often called Poynting's theorem [9]. The instantaneous Poynting vector can be calculated as

$$\mathbf{S} = \mathbf{E}_{\text{inst}} \times \mathbf{H}_{\text{inst}},\tag{9}$$

We are interested in the time-averaged Poynting vector and it can be derived as:

$$\begin{aligned}\langle \mathbf{S} \rangle &= \frac{1}{T} \int_0^T \mathbf{S}(t) dt \\ &= \frac{1}{T} \int_0^T \mathbf{E}_{\text{inst}}(t) \times \mathbf{H}_{\text{inst}}(t) dt \\ &= \frac{1}{T} \int_0^T \text{Re}(\mathbf{E}e^{j\omega t}) \times \text{Re}(\mathbf{H}e^{j\omega t}) dt \\ &= \frac{1}{T} \int_0^T \frac{1}{2}(\mathbf{E}e^{j\omega t} + \mathbf{E}^*e^{-j\omega t}) \times \frac{1}{2}(\mathbf{H}e^{j\omega t} + \mathbf{H}^*e^{-j\omega t}) dt \\ &= \frac{1}{2}\text{Re}(\mathbf{E} \times \mathbf{H}^*),\end{aligned}\tag{10}$$

which is Equation (27) in the main paper. The time-averaged Poynting vector is equivalent to vector irradiance in radiometry and it provides a way to compute the azimuthal distribution from the scattered field. In a linearly polarized plane wave of a certain frequency, the Poynting vector always points in the propagation direction while oscillating in magnitude. The magnitude of the time-averaged Poynting vector for a plane wave is:

$$|\langle \mathbf{S} \rangle| = \frac{1}{2} \sqrt{\frac{\epsilon}{\mu}} |\mathbf{E}|^2.\tag{11}$$

3 Dielectric cylinder scattering problems

In this work, we propose the first fiber scattering model that is built on wave optics simulation in computer graphics. Conducting full wave scattering simulations is expensive, as it requires resolving both electromagnetic fields and geometry at well below the scale of visible light wavelengths. Furthermore, creating a complete scattering model requires many simulations to account for all possible illumination directions. This work shows a way to make this computation tractable through a series of simplifications:

- Like most fiber scattering models we assume a separable form for the model, as a product of longitudinal and azimuthal scattering distributions, and in this paper we derive new azimuthal distributions, while adopting a longitudinal model from prior work [5].
- For modeling azimuthal scattering we assume that fibers are extrusions with perfect translational symmetry. We exploit this symmetry in a “2.5D” wave scattering simulation that computes 3D electromagnetic fields using values only in a 2D cross-sectional slice.
- To avoid the need to discretize the volume of the fiber and the space surrounding it, we employ a boundary integral formulation that reduces the set of unknowns to a 1D discretization of the fiber’s planar cross section curve.

With careful attention to efficiency in implementation, this makes it possible to compute azimuthal scattering for fibers of arbitrary cross sections and arbitrary material properties, for all incident and scattered directions and all relevant wavelengths, in a precomputation, resulting in tabulated azimuthal scattering functions to be used in rendering.

In this section, we describe how to solve the infinitely long dielectric cylinder scattering problem using the Boundary Element Method (BEM) for arbitrary cross-section shaped cylinders and using the Lorenz-Mie theory for circular cross-section shaped cylinders.

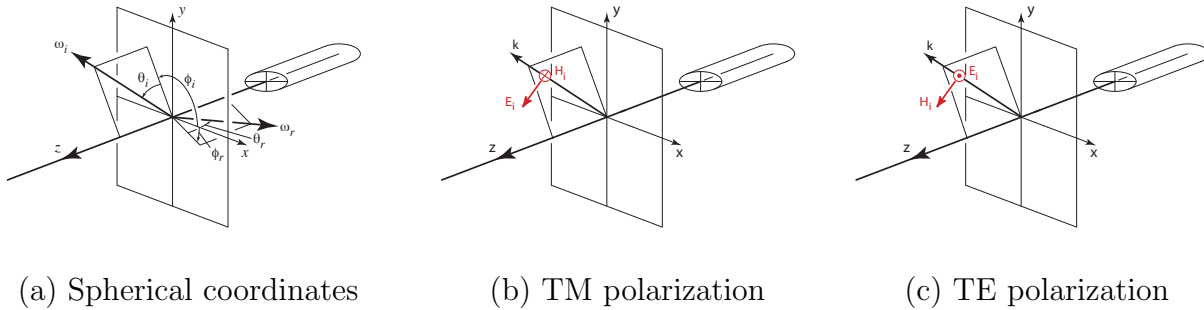


Figure 1: (a) An illustration of the commonly adopted longitudinal-azimuthal parameterization for fiber scattering models. Each of the directions ω_i and ω_r in 3D is parameterized using the polar angle θ , defined as the angle between ω and the xy -plane (the plane perpendicular to the cylinder axis), and the azimuthal angle ϕ , defined in xy -plane. (b) and (c) illustrate the transverse-magnetic (TM) and transverse-electric (TE) polarization types that can be linearly combined to produce arbitrary polarization configuration.

3.1 Problem setup

The boundary of the fiber is the extrusion of a curve Γ in the x - y plane along the z axis. This surface divides space into exterior and interior regions, denoted 1 and 2 respectively, with different material properties (ϵ_1, μ_1) and (ϵ_2, μ_2) . For a dielectric fiber with refractive index $n + j\kappa$ surrounded by free space, $\epsilon_1 = \epsilon_0$, $\epsilon_2 = (n + j\kappa)^2\epsilon_0$, and $\mu_1 = \mu_2 = \mu_0$, where ϵ_0 and μ_0 are the permittivity and permeability of free space.

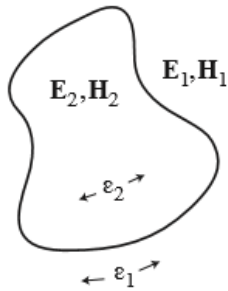


Figure 2: Introducing a fiber divides the space the two regions. We illustrate a fiber cross section and denote the exterior and interior regions as region 1 and 2 respectively. The dielectric cylinder scattering problem has fields both interior and exterior to the fiber with a change in material properties (ϵ) at the surface.

Fields The fiber is illuminated by a plane wave propagating in direction $-\omega_i$. As illustrated in Figure 1 (b) and (c), there are two types of polarization. One is called transverse-magnetic (TM), where the magnetic field \mathbf{H}_i is perpendicular to the plane defined by the cylinder axis and wave propagation direction (Figure 1 (b)); the other polarization type is called transverse-electric (TE), where the electric field \mathbf{E}_i is perpendicular the plane defined by the cylinder axis and wave propagation direction (Figure 1 (c)). Note that any other linearly polarized incidence wave can be expressed as a linear combination of TM and TE incidence. For simplicity of integrating the new scattering model into current rendering systems we assume light incident on a fiber is always unpolarized. Therefore, we compute the scattering distributions for TM and TE polarization and take the mean of the two, and this produces the scattering distribution for an unpolarized incident wave. Note that oblique incidence cylinder scattering with one type of polarization will result in scattered fields with a mixed of two types of polarization.

Using linearity, scattering from other kinds of illumination can be handled by first expressing them as sums of plane waves. We take the Gaussian beam incidence field as an example to explain this in Section 4.

The presence of the fiber alters the fields and we call the resulting fields the *total fields* $\mathbf{E}_t, \mathbf{H}_t$. In the rest of this document, we will express the total fields as sums of simpler fields $\mathbf{E}_1, \mathbf{H}_1$, which are zero in the interior of the fiber, and $\mathbf{E}_2, \mathbf{H}_2$, which are zero in the exterior. We further subdivide the exterior total fields into the incident fields and the *scattered fields* $\mathbf{E}_s, \mathbf{H}_s$ such that

$$\mathbf{E}_t = \mathbf{E}_1 + \mathbf{E}_2; \quad \mathbf{H}_t = \mathbf{H}_1 + \mathbf{H}_2 \quad (12)$$

$$\mathbf{E}_1 = \mathbf{E}_i + \mathbf{E}_s; \quad \mathbf{H}_1 = \mathbf{H}_i + \mathbf{H}_s \quad (13)$$

The scattered fields propagate outward from the fiber and will be the key to computing the BCSDf for rendering. The scattered wave in region 1 travels with the same speed as the incident wave (free space light speed c) and the transmitted wave in region 2 travels with speed c/η .

Boundary conditions One can derive the boundary conditions at the interface between the interior and the exterior of the fiber from the integral equivalents of the Maxwell equations [9]. Let $\mathbf{E}_1, \mathbf{H}_1$ and $\mathbf{E}_2, \mathbf{H}_2$ denote the total fields exterior and interior to the cylinder. On the surface the tangential electric and magnetic fields are continuous

$$\hat{\mathbf{n}} \times \mathbf{E}_1 = \hat{\mathbf{n}} \times \mathbf{E}_2; \quad \hat{\mathbf{n}} \times \mathbf{H}_1 = \hat{\mathbf{n}} \times \mathbf{H}_2. \quad (14)$$

3.2 Boundary integrals and Boundary Element Method (BEM)

We use the Boundary Element Method (BEM) to numerically solve the dielectric cylinder scattering problem. Compared to the other numerical methods, BEM has lower complexity as it only needs to discretize the boundary of the object. The method is outlined as the following:

- We first make use of the surface equivalence principle [10, 13] to turn the scattering problem that contains different materials into equivalent exterior and interior problems, where there is only one kind of material in each problem and the fields can be characterized by Helmholtz equations.
- We then derive general 3D source-field relations that write the scattered fields as the integration of the sources with the appropriate Green's function.
- Next, we make use of the translational symmetry of the dielectric cylinder problem that lets us model fibers locally as homogeneous infinitely long cylinders and turn 3D source-field relations into 2.5D ones.
- We then form the boundary integral equations by applying the boundary conditions and the relation between incident, scattered and total fields.
- Finally, we solve the boundary integral equations using BEM, which discretizes the boundary of the cylinder cross section and turns the boundary integral equations into a linear system to solve.

3.2.1 Splitting the problem via surface equivalence

Different source distributions outside a given region can produce the same field inside the region and we say the two sources that produce the same field are equivalent. The surface equivalence principle [10, 13] states that fields \mathbf{E}, \mathbf{H} that exist in a source-free region can be generated by surface currents \mathbf{J}, \mathbf{M} residing on the region's boundary. This equivalence lets us transform our scattering problem into a pair of problems concerning unbounded homogeneous media, which are amenable to solution using Green's functions (Figure 1).

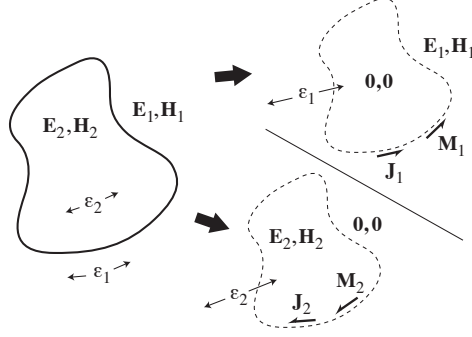


Figure 3: Separation of interior and exterior fields via surface equivalence. The original problem (left) has fields both interior and exterior to the fiber with a change in material properties at the surface. It is transformed into a pair of problems (right), each in a homogeneous medium, with surface currents generating the field on one side and zero on the other side.

The two equivalent problems are called the equivalent exterior problem (Figure 3 right) and the equivalent interior problem (Figure 3 middle). In the exterior (interior) problem, the fields is split into two components with original fields in region 1 (region 2) and null fields in region 2 (region 1). The electromagnetic fields are discontinuous across the interfaces and this is achieved by introducing the fictitious surface currents. In the exterior problem, the fictitious electric and magnetic currents are \mathbf{J}_1 and \mathbf{M}_1 and the condition for the jump of fields is

$$\mathbf{M}_1 = -\hat{\mathbf{n}}_1 \times \mathbf{E}_1, \quad \mathbf{J}_1 = \hat{\mathbf{n}}_1 \times \mathbf{H}_1. \quad (15)$$

In the interior problem, the fictitious currents are \mathbf{J}_2 and \mathbf{M}_2 and the condition is

$$\mathbf{M}_2 = -\hat{\mathbf{n}}_2 \times \mathbf{E}_2, \quad \mathbf{J}_2 = \hat{\mathbf{n}}_2 \times \mathbf{H}_2, \quad (16)$$

where $\hat{\mathbf{n}}_1 = \hat{\mathbf{n}}$ is the surface normal vector pointing towards region 1. Then we can modify the material parameters in regions where we have null fields because this will not affect the fields. In particular, we set the material properties to match those in the other region, transforming our problem into two (linked) homogeneous problems. The two equivalent problems are related via the boundary conditions of the original problem (14) and it requires

$$\mathbf{J} = \mathbf{J}_1 = -\mathbf{J}_2; \quad \mathbf{M} = \mathbf{M}_1 = -\mathbf{M}_2. \quad (17)$$

In regions of space where permittivity ϵ and permeability μ are constant, Maxwell's equations reduce to the Helmholtz equations [9].

$$\begin{aligned} \nabla^2 \mathbf{E} + k^2 \mathbf{E} &= j\omega\mu \mathbf{J} - \frac{1}{j\omega\epsilon} \nabla(\nabla \cdot \mathbf{J}) + \nabla \times \mathbf{M} = j\omega\mu \left(1 + \frac{1}{k^2} \nabla \nabla \cdot\right) \mathbf{J} + \nabla \times \mathbf{M} \\ \nabla^2 \mathbf{H} + k^2 \mathbf{H} &= j\omega\epsilon \mathbf{M} - \frac{1}{j\omega\mu} \nabla(\nabla \cdot \mathbf{M}) - \nabla \times \mathbf{J} = j\omega\epsilon \left(1 + \frac{1}{k^2} \nabla \nabla \cdot\right) \mathbf{M} - \nabla \times \mathbf{J} \end{aligned} \quad (18)$$

which we can use to compute the fields generated by a set of currents. In particular from \mathbf{J}_1 and \mathbf{M}_1 we can compute the scattered fields $\mathbf{E}_s, \mathbf{H}_s$ and from \mathbf{J}_2 and \mathbf{M}_2 we can compute the

fields $\mathbf{E}_2, \mathbf{H}_2$ (using the material parameters for regions 1 and 2 respectively). Therefore we use the currents to parameterize the fields in solving for them. In the following subsection, we will explain how to convert the above PDEs into integral equations with a Green's function. The resulting equations are called *source field relations*. The fields will then be expressed in terms of the sources in integral equations. The source field relations further enable the boundary integral formulation of the scattering problem. The boundary integral formulation is easier to solve comparing to the PDEs because sources are supported by a finite domain while fields in PDEs exists in the entire space.

3.2.2 Source field relations in 3D

The 3D scalar Green's function [12] represents the scalar field at \mathbf{r} produced by a point source at \mathbf{r}' . It satisfies

$$\nabla^2 G(\mathbf{r}, \mathbf{r}') + k^2 G(\mathbf{r}, \mathbf{r}') = -\delta(\mathbf{r}, \mathbf{r}'). \quad (19)$$

The Green's function for this equation is not uniquely defined but we want the one corresponds to a physically plausible solution (i.e. the one in which the scattered power flows purely outward as defined by the Sommerfeld radiation condition [14]). The 3D Green's function is

$$G(\mathbf{r}, \mathbf{r}') = \frac{e^{-jk|\mathbf{r}-\mathbf{r}'|}}{4\pi|\mathbf{r}-\mathbf{r}'|}. \quad (20)$$

We can write (18) compactly as

$$\begin{aligned} \mathcal{P}\mathbf{E}(\mathbf{r}) &= f_1(\mathbf{r}) \\ \mathcal{P}\mathbf{H}(\mathbf{r}) &= f_2(\mathbf{r}) \end{aligned} \quad (21)$$

with linear operator $\mathcal{P}(\cdot) = (\nabla^2 + k^2)(\cdot)$ acting on \mathbf{r} and the forcing functions f_1, f_2 are

$$\begin{aligned} f_1(\mathbf{r}) &= j\omega\mu\left(1 + \frac{1}{k^2}\nabla\nabla\cdot\right)\mathbf{J}(\mathbf{r}) + \nabla \times \mathbf{M}(\mathbf{r}), \\ f_2(\mathbf{r}) &= j\omega\epsilon\left(1 + \frac{1}{k^2}\nabla\nabla\cdot\right)\mathbf{M}(\mathbf{r}) - \nabla \times \mathbf{J}(\mathbf{r}). \end{aligned} \quad (22)$$

Using the Green's function definition in (19)

$$\int \mathcal{P}G(\mathbf{r}, \mathbf{r}')f_1(\mathbf{r}')d\mathbf{r}' = \int -\delta(\mathbf{r}, \mathbf{r}')f_1(\mathbf{r}')d\mathbf{r}' = -f_1(\mathbf{r}) \quad (23)$$

We have

$$\mathcal{P}\left(\int G(\mathbf{r}, \mathbf{r}')f_1(\mathbf{r}')d\mathbf{r}'\right) = -f_1(\mathbf{r}) \quad \Rightarrow \quad \mathbf{E}(\mathbf{r}) = -\int G(\mathbf{r}, \mathbf{r}')f_1(\mathbf{r}')d\mathbf{r}'. \quad (24)$$

Similarly,

$$\mathbf{H}(\mathbf{r}) = -\int G(\mathbf{r}, \mathbf{r}')f_2(\mathbf{r}')d\mathbf{r}'. \quad (25)$$

We call the above two equations the *source field relations in 3D* as they relate the fields with the currents in 3D via integral equations. Next we will show we can make use of the symmetry of our problem to reduce it 2.5D.

3.2.3 Source field relations in 2.5D

We adopt the coordinate system shown in Figure 1 (a), and represent the 3D and 2D coordinates using $\mathbf{r} = x\hat{\mathbf{x}} + y\hat{\mathbf{y}} + z\hat{\mathbf{z}}$ and $\boldsymbol{\rho} = x\hat{\mathbf{x}} + y\hat{\mathbf{y}}$. The incident field can be expressed as

$$\mathbf{E}_i = \mathbf{E}_0 e^{j\mathbf{k}_\rho \cdot \boldsymbol{\rho}} e^{jk_z z}, \quad \mathbf{H}_i = \mathbf{H}_0 e^{j\mathbf{k}_\rho \cdot \boldsymbol{\rho}} e^{jk_z z} \quad (26)$$

where $\mathbf{k} = \mathbf{k}_\rho + k_z \hat{\mathbf{z}}$ and $k_\rho = |\mathbf{k}_\rho|$. Since the z dependence of this source field is a complex exponential, a translation in z corresponds to multiplying the field by a global scalar phase factor. Since (18) is a linear PDE, scaling the source will scale all the quantities in the problem by the same factor; hence all the fields and currents inherit the same z dependence as $\mathbf{E}_i, \mathbf{H}_i$:

$$\begin{aligned} \mathbf{E}(\mathbf{r}) &= \mathbf{E}(\boldsymbol{\rho}) e^{jk_z z}, & \mathbf{H}(\mathbf{r}) &= \mathbf{H}(\boldsymbol{\rho}) e^{jk_z z}, \\ \mathbf{J}(\mathbf{r}) &= \mathbf{J}(\boldsymbol{\rho}) e^{jk_z z}, & \mathbf{M}(\mathbf{r}) &= \mathbf{M}(\boldsymbol{\rho}) e^{jk_z z}. \end{aligned} \quad (27)$$

Applying to the source field relations in 3D, we get

$$\begin{aligned} \mathbf{E}(\mathbf{r}) &= \mathbf{E}(\boldsymbol{\rho}) e^{jk_z z} = - \int G(\mathbf{r}, \mathbf{r}') f_1(\mathbf{r}') d\mathbf{r}' = - \int \left(\int G(\mathbf{r}, \mathbf{r}') e^{jk_z z'} dz' \right) f_1(\boldsymbol{\rho}') d\boldsymbol{\rho}', \\ \mathbf{H}(\mathbf{r}) &= \mathbf{H}(\boldsymbol{\rho}) e^{jk_z z} = - \int G(\mathbf{r}, \mathbf{r}') f_2(\mathbf{r}') d\mathbf{r}' = - \int \left(\int G(\mathbf{r}, \mathbf{r}') e^{jk_z z'} dz' \right) f_2(\boldsymbol{\rho}') d\boldsymbol{\rho}', \end{aligned} \quad (28)$$

where

$$\int G(\mathbf{r}, \mathbf{r}') e^{jk_z z'} dz' = \frac{1}{4j} H_0^{(2)}(k_\rho |\boldsymbol{\rho} - \boldsymbol{\rho}'|) e^{jk_z z}, \quad (29)$$

and $G(\boldsymbol{\rho}, \boldsymbol{\rho}') = \frac{1}{4j} H_0^{(2)}(k_\rho |\boldsymbol{\rho} - \boldsymbol{\rho}'|)$ is the 2D Green's function that represents the field at $\boldsymbol{\rho}$ produced by a line source at $\boldsymbol{\rho}'$. $H_0^{(2)}$ is the zeroth order Hankel function of the second kind. It satisfies the following equation with the radiation condition:

$$\nabla^2 G(\boldsymbol{\rho}, \boldsymbol{\rho}') + k_\rho^2 G(\boldsymbol{\rho}, \boldsymbol{\rho}') = -\delta(\boldsymbol{\rho}, \boldsymbol{\rho}'). \quad (30)$$

After integrating out z' (28) can be written as

$$\begin{aligned} \mathbf{E}(\boldsymbol{\rho}) e^{jk_z z} &= - \int e^{jk_z z} G(\boldsymbol{\rho}, \boldsymbol{\rho}') f_1(\boldsymbol{\rho}') d\boldsymbol{\rho}', \\ \mathbf{H}(\boldsymbol{\rho}) e^{jk_z z} &= - \int e^{jk_z z} G(\boldsymbol{\rho}, \boldsymbol{\rho}') f_2(\boldsymbol{\rho}') d\boldsymbol{\rho}'. \end{aligned} \quad (31)$$

Without loss of generality, we take $z = 0$. After some algebraic manipulations we arrive at equations (13) and (14) in the main paper:

$$\begin{aligned} \mathbf{E}(\boldsymbol{\rho}) &= -j\omega\mu\mathcal{L}\mathbf{J}(\boldsymbol{\rho}) - \mathcal{K}\mathbf{M}(\boldsymbol{\rho}), \\ \mathbf{H}(\boldsymbol{\rho}) &= -j\omega\epsilon\mathcal{L}\mathbf{M}(\boldsymbol{\rho}) + \mathcal{K}\mathbf{J}(\boldsymbol{\rho}). \end{aligned} \quad (32)$$

where

$$(\mathcal{L}\mathbf{X})(\boldsymbol{\rho}) = \left[1 + \frac{1}{k^2} \nabla \nabla \cdot \right] \int_{\Gamma} e^{jk_z z} G(\boldsymbol{\rho}, \boldsymbol{\rho}') \mathbf{X}(\boldsymbol{\rho}') d\boldsymbol{\rho}' \Big|_{z=0}, \quad (33)$$

$$(\mathcal{K}\mathbf{X})(\boldsymbol{\rho}) = \nabla \times \int_{\Gamma} e^{jk_z z} G(\boldsymbol{\rho}, \boldsymbol{\rho}') \mathbf{X}(\boldsymbol{\rho}') d\boldsymbol{\rho}' \Big|_{z=0}. \quad (34)$$

The ∇ operator and \mathbf{X} can be decomposed as

$$\nabla = \nabla_{\rho} + \hat{\mathbf{z}} \frac{\partial}{\partial z} = \nabla_{\rho} + jk_z \hat{\mathbf{z}}, \quad (35)$$

$$\mathbf{X} = \mathbf{X}_{\rho} + X_z \hat{\mathbf{z}}. \quad (36)$$

3.2.4 Boundary integral equations

Now we can form the boundary integral equations governing the scattering problem. Combining the boundary current constraints (15), (16) and the relation between the incident fields, scattered fields and the total fields (13), we get

$$\begin{aligned} \mathbf{M} &= -\hat{\mathbf{n}}_1 \times (\mathbf{E}_i + \mathbf{E}_s), & \mathbf{J} &= \hat{\mathbf{n}}_1 \times (\mathbf{H}_i + \mathbf{H}_s) \\ \mathbf{M} &= \hat{\mathbf{n}}_2 \times \mathbf{E}_2, & \mathbf{J} &= -\hat{\mathbf{n}}_2 \times \mathbf{H}_2 \end{aligned} \quad (37)$$

where the top two equations are for the exterior problem and the bottom two equations are for the interior problem. The source field relations relates $\mathbf{E}_s, \mathbf{H}_s, \mathbf{E}_2, \mathbf{H}_2$ with \mathbf{J}, \mathbf{M} :

$$\begin{aligned} \mathbf{E}_s(\boldsymbol{\rho}) &= -j\omega\mu_1 \mathcal{L}_1 \mathbf{J}(\boldsymbol{\rho}) - \mathcal{K}_1 \mathbf{M}(\boldsymbol{\rho}), \\ \mathbf{H}_s(\boldsymbol{\rho}) &= -j\omega\epsilon_1 \mathcal{L}_1 \mathbf{M}(\boldsymbol{\rho}) + \mathcal{K}_1 \mathbf{J}(\boldsymbol{\rho}), \\ \mathbf{E}_2(\boldsymbol{\rho}) &= -j\omega\mu_2 \mathcal{L}_2 \mathbf{J}(\boldsymbol{\rho}) - \mathcal{K}_2 \mathbf{M}(\boldsymbol{\rho}), \\ \mathbf{H}_2(\boldsymbol{\rho}) &= -j\omega\epsilon_2 \mathcal{L}_2 \mathbf{M}(\boldsymbol{\rho}) + \mathcal{K}_2 \mathbf{J}(\boldsymbol{\rho}). \end{aligned} \quad (38)$$

where \mathcal{L}_1 (resp. \mathcal{L}_2) is the \mathcal{L} operator defined using the wavenumber for region 1 (resp. 2), and similarly for \mathcal{K}_1 and \mathcal{K}_2 . Combining (37) and (38) we get the electric field integral equations (EFIE):

$$\begin{aligned} \mathbf{M}(\boldsymbol{\rho}) + \hat{\mathbf{n}}_1(\boldsymbol{\rho}) \times [-j\omega\mu_1 (\mathcal{L}_1 \mathbf{J})(\boldsymbol{\rho}) - (\mathcal{K}_1 \mathbf{M})(\boldsymbol{\rho})] &= -\hat{\mathbf{n}}_1(\boldsymbol{\rho}) \times \mathbf{E}_i(\boldsymbol{\rho}) \\ \mathbf{M}(\boldsymbol{\rho}) + \hat{\mathbf{n}}_2(\boldsymbol{\rho}) \times [-j\omega\mu_2 (\mathcal{L}_2 \mathbf{J})(\boldsymbol{\rho}) - (\mathcal{K}_2 \mathbf{M})(\boldsymbol{\rho})] &= \mathbf{0}, \end{aligned} \quad (39)$$

and the magnetic field integral equations (MFIE):

$$\begin{aligned} \mathbf{J}(\boldsymbol{\rho}) - \hat{\mathbf{n}}_1(\boldsymbol{\rho}) \times [-j\omega\epsilon_1 (\mathcal{L}_1 \mathbf{M})(\boldsymbol{\rho}) + (\mathcal{K}_1 \mathbf{J})(\boldsymbol{\rho})] &= \hat{\mathbf{n}}_1(\boldsymbol{\rho}) \times \mathbf{H}_i(\boldsymbol{\rho}) \\ \mathbf{J}(\boldsymbol{\rho}) - \hat{\mathbf{n}}_2(\boldsymbol{\rho}) \times [-j\omega\epsilon_2 (\mathcal{L}_2 \mathbf{M})(\boldsymbol{\rho}) + (\mathcal{K}_2 \mathbf{J})(\boldsymbol{\rho})] &= \mathbf{0}, \end{aligned} \quad (40)$$

Equations (39) and (40) constitute four equations in two unknowns. Here, we combine them so as to ensure their solution is unique. The specific combination strategy adopted here is the PMCHWT approach [11], which subtracts the second equation from the first equation in each of Equations (39) and (40), resulting in the smaller system

$$\begin{aligned} \hat{\mathbf{n}} \times [-j\omega(\mu_1 \mathcal{L}_1 + \mu_2 \mathcal{L}_2) \mathbf{J} - (\mathcal{K}_1 + \mathcal{K}_2) \mathbf{M}] &= -\hat{\mathbf{n}} \times \mathbf{E}_1^i \\ -\hat{\mathbf{n}} \times [-j\omega(\epsilon_1 \mathcal{L}_1 + \epsilon_2 \mathcal{L}_2) \mathbf{M} + (\mathcal{K}_1 + \mathcal{K}_2) \mathbf{J}] &= \hat{\mathbf{n}} \times \mathbf{H}_1^i. \end{aligned} \quad (41)$$

3.2.5 Boundary Element Method (BEM)

With the boundary integral equations we derived above, we apply BEM to numerically solve them. We solve for the unknown currents by applying a Galerkin-type method to convert Equation (41) into a linear system [12]. First, we discretize the fiber cross-section boundary Γ into N line segments and represent both the electric and magnetic surface currents using the same set of $2N$ linear basis functions \mathbf{f} :

$$\mathbf{J}(\boldsymbol{\rho}) \approx \sum_{i=1}^{2N} (I_J)_i \mathbf{f}_i(\boldsymbol{\rho}), \quad \mathbf{M}(\boldsymbol{\rho}) \approx \sum_{i=1}^{2N} (I_M)_i \mathbf{f}_i(\boldsymbol{\rho}) \quad (42)$$

Each basis function is supported over two adjacent elements. The first N of the $2N$ basis functions represent z -directed currents, while the other N represent currents that flow on the fiber surface orthogonal to z .

Substituting the approximation (42) into the system (41) and testing the resulting equations using the same basis \mathbf{f} leads to a matrix equation

$$\begin{bmatrix} Z_{ME} & Z_{JE} \\ Z_{MH} & Z_{JH} \end{bmatrix} \begin{bmatrix} I_M \\ I_J \end{bmatrix} = \begin{bmatrix} V_E \\ V_H \end{bmatrix}. \quad (43)$$

where the submatrices are formed from inner products of testing functions with the components of (41)

$$\begin{aligned} (Z_{ME})_{ik} &= -\langle \mathbf{f}_i, \hat{\mathbf{n}} \times ((\mathcal{K}_1 + \mathcal{K}_2) \mathbf{f}_k) \rangle \\ (Z_{JE})_{ik} &= -j\omega \langle \mathbf{f}_i, \hat{\mathbf{n}} \times ((\mu_1 \mathcal{L}_1 + \mu_2 \mathcal{L}_2) \mathbf{f}_k) \rangle \\ (Z_{MH})_{ik} &= j\omega \langle \mathbf{f}_i, \hat{\mathbf{n}} \times ((\epsilon_1 \mathcal{L}_1 + \epsilon_2 \mathcal{L}_2) \mathbf{f}_k) \rangle \\ (Z_{JH})_{ik} &= -\langle \mathbf{f}_i, \hat{\mathbf{n}} \times ((\mathcal{K}_1 + \mathcal{K}_2) \mathbf{f}_k) \rangle \\ (V_E)_i &= \langle \mathbf{f}_i, -\hat{\mathbf{n}} \times \mathbf{E}_i \rangle \\ (V_H)_i &= \langle \mathbf{f}_i, \hat{\mathbf{n}} \times \mathbf{H}_i \rangle. \end{aligned} \quad (44)$$

Here we define the inner product between a pair of vector functions \mathbf{a} and \mathbf{b} as

$$\langle \mathbf{a}, \mathbf{b} \rangle = \int_{\Gamma} \mathbf{a}(s) \cdot \mathbf{b}(s) ds \quad (45)$$

This block matrix system has a total dimension $4N \times 4N$. Z_{ME} represents the block where we express \mathbf{M} in EFIE (E) using the basis functions \mathbf{f} and apply the same set of basis functions as testing functions. The other blocks are named analogously. V_E and V_H are the test integrals on the incident electric field and magnetic field. Finally, we solve for the coefficients I_M and I_J , and we obtain from (42) the surface currents $\mathbf{J}(\boldsymbol{\rho})$ and $\mathbf{M}(\boldsymbol{\rho})$, which are the equivalent surface sources that define the solution to our scattering problem.

Regarding the implementation of Equation (44), we would like to note that:

- The differential operators in \mathcal{L} and \mathcal{K} can be rearranged to operate on the basis functions to simplify the computation. Since each basis function is supported over two adjacent elements and is zero elsewhere, it is convenient to define the basis function locally instead of globally and conduct the integration with local support.

- The evaluation of the integral is done by Gaussian quadrature except for the cases when the inner integral and outer integral integrate on the same line segment.
- When the inner integral and the outer integral integrate on the same element, the integral contains the contribution from $G(\boldsymbol{\rho}, \boldsymbol{\rho}')$ where $\boldsymbol{\rho} = \boldsymbol{\rho}'$ and G is singular. In this case, we apply the small argument approximation of the Hankel function [6]

$$H_0^{(2)}(kx) \approx 1 - j\frac{2}{\pi} \log\left(\frac{1.1781kx}{2}\right), \quad x \rightarrow 0, \quad (46)$$

and the integral can be computed analytically.

3.2.6 Computing far-field quantities

Having computed the surface currents, we can use the source field relations (Equation (32)) to compute the scattered electric field (\mathbf{E}_s) and the scattered magnetic field (\mathbf{H}_s) on an observing circle with radius R . The quantity of interest is the azimuthal scattering function, which describes the distribution of scattered light within the specular cone. As introduced in Section 2, the time-averaged Poynting vector,

$$\langle \mathbf{S} \rangle = \frac{1}{2} \text{Re}(\mathbf{E} \times \mathbf{H}^*), \quad (47)$$

is equivalent to vector irradiance in radiometry. It provides a way to compute the azimuthal distribution from the scattered field.

The quantities we can compute from the simulation include the angular distribution of scattered intensity per unit length and the absorbed power per unit length.

Scattered intensity The scattered wave is an outward propagating wave. In the far field, the scattered wave is locally a plane wave, traveling in the direction $\hat{\mathbf{e}}_s(\phi_r) = \cos\theta_i \hat{\boldsymbol{\rho}}(\phi_r) - \sin\theta_i \hat{\mathbf{z}}$, where $\hat{\boldsymbol{\rho}}(\phi_r)$ is the unit vector in the $x - y$ plane, pointing away from the origin and forming an angle of ϕ_r with the x-axis. The surface of constant phase, or *wave fronts* of the scattered wave, forms a cone surface.

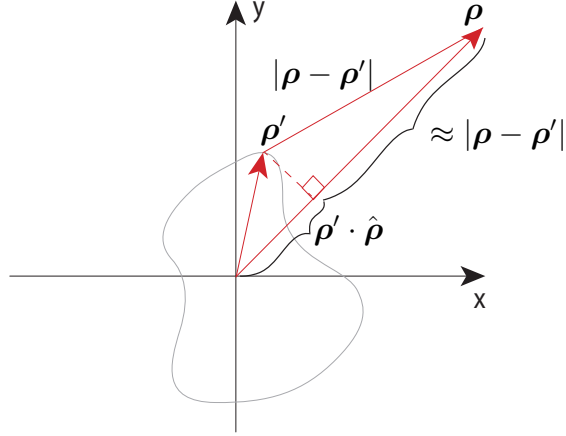
When we use Equation (32) to compute the scattered field in the far field, we can apply the asymptotic forms of the 2D Green's function. In the far field, the limiting expression for the Hankel function is [1]

$$\lim_{k|\boldsymbol{\rho}-\boldsymbol{\rho}'|\rightarrow\infty} H_0^{(2)}(k|\boldsymbol{\rho}-\boldsymbol{\rho}'|) = \sqrt{\frac{2j}{\pi k|\boldsymbol{\rho}-\boldsymbol{\rho}'|}} e^{-jk|\boldsymbol{\rho}-\boldsymbol{\rho}'|} \quad (48)$$

Denote $\rho = |\boldsymbol{\rho}|$. When $|\boldsymbol{\rho}| \gg |\boldsymbol{\rho}'|$, we have $|\boldsymbol{\rho} - \boldsymbol{\rho}'| \approx \rho$ and $|\boldsymbol{\rho} - \boldsymbol{\rho}'| \approx \rho - \boldsymbol{\rho}' \cdot \hat{\boldsymbol{\rho}}$. The following figure illustrates this approximation. Thus we have

$$\lim_{k|\boldsymbol{\rho}-\boldsymbol{\rho}'|\rightarrow\infty} H_0^{(2)}(k|\boldsymbol{\rho}-\boldsymbol{\rho}'|) = \sqrt{\frac{2j}{\pi k\rho}} e^{-jk\rho} e^{jk\boldsymbol{\rho}' \cdot \hat{\boldsymbol{\rho}}}, \quad (49)$$

and this can be used to compute the scattered fields in the far field.



Applying the Poynting vector, the scattered intensity per unit length in the far field can be calculated as

$$I_s(\theta_i, \phi_i, \phi_r, \lambda) = \frac{1}{2} \text{Re}(\mathbf{E}_{s_{\text{far}}} \times \mathbf{H}_{s_{\text{far}}}^*) \cdot \boldsymbol{\rho}(\phi_r), \quad (50)$$

where $\boldsymbol{\rho}(\phi_r)$ is the vector in the $x - y$ plane, pointing away from the origin and forming an angle of ϕ_r with the x -axis, with $|\boldsymbol{\rho}(\phi_r)|$ much greater than the fiber radius. The total scattered power per unit length, W_s , can be obtained by integrating $I_s(\phi_r)$.

Absorption Absorbed power per unit length can be calculated by integrating the normal component of the total field's Poynting vector over the boundary, as the net flow at the boundary is the absorption:

$$\begin{aligned} W_a &= \int_{\Gamma} \frac{1}{2} \text{Re}(\mathbf{E}_1 \times \mathbf{H}_1^*) \cdot \hat{\mathbf{n}}_1(s) ds \\ &= \int_{\Gamma} \frac{1}{2} \text{Re}(\mathbf{J}_1^* \times \mathbf{M}_1) \cdot \hat{\mathbf{n}}_1(s) ds. \end{aligned} \quad (51)$$

The second equation is derived by applying Equation (15).

3.3 Lorenz-Mie theory

In Section 3.2, we describe how to use BEM to solve the cylinder scattering problem with arbitrary cross-section shapes. Although BEM has lower complexity than other numerical methods, it is still expensive as it involves large matrix assembly and solves. In this subsection we will summarize how to apply Lorenz-Mie theory to solve for infinite circular scattering problem, which is a special case of the arbitrary cross section cylinder scattering problem. Mie theory provides an analytic solution to this specific problem and is much more efficient to compute [2].

Assuming the infinitely long cylinder does not have variation along the cylinder axis, Mie theory derives the scattered fields everywhere in the space under plane wave incidence. It starts with the solution of the scalar wave equation

$$\nabla^2 \psi + k^2 \psi = 0. \quad (52)$$

In cylindrical polar coordinates r, ϕ, z , the scalar wave equation is

$$\frac{1}{r} \frac{\partial}{\partial r} \left(r \frac{\partial \psi}{\partial r} \right) + \frac{1}{r^2} \frac{\partial^2 \psi}{\partial \phi^2} + \frac{\partial^2 \psi}{\partial z^2} + k^2 \psi = 0. \quad (53)$$

The separable solutions $\psi_n(r, \phi, z)$ to the above equation are in terms of the solutions to the Bessel equation. The vector cylindrical harmonics generated by ψ_n are

$$\mathbf{P}_n = \nabla \times (\hat{\mathbf{z}} \psi_n), \quad \mathbf{Q}_n = \frac{\nabla \times \mathbf{P}_n}{k}. \quad (54)$$

Then we can write the incident field in the expansion of the generating functions \mathbf{P}_n s and \mathbf{Q}_n s with appropriate Bessel functions. With plane wave incidence we can compute the desired coefficients in the expansion. Next, we express the total fields inside the cylinder and the scattered fields in terms of generating functions with appropriate Bessel function so that the continuity conditions at the boundary can be satisfied, the field at the origin is finite and the scattered field is an outgoing wave. Finally, by applying the boundary conditions upon scattering we can solve for all the coefficients in the expansions. The relation between the scattered field to the incident field is shown in the equation below. At distance R , the scattered electric field can be written as:

$$\begin{pmatrix} E_{\parallel s} \\ E_{\perp s} \end{pmatrix} = e^{j3\pi/4} \sqrt{\frac{2}{\pi k R \cos \theta}} e^{jk(R \cos \theta - z \sin \theta)} \begin{pmatrix} T_1 & T_4 \\ T_3 & T_2 \end{pmatrix} \begin{pmatrix} E_{\parallel i} \\ E_{\perp i} \end{pmatrix}, \quad (55)$$

where \parallel denotes TM polarization, i.e. the electric field is in the plane defined by the wave vector and the cylinder axis; \perp denotes TE polarization, i.e. the electric field is perpendicular

to the plane defined by the wave vector and the cylinder axis; and

$$\begin{aligned}
T_1 &= \sum_{-\infty}^{\infty} b_{nI} e^{-jn(\pi-\phi)} = b_{0I} + 2 \sum_{n=1}^{\infty} b_{nI} \cos(n(\pi - \phi)), \\
T_2 &= \sum_{-\infty}^{\infty} a_{nII} e^{-jn(\pi-\phi)} = a_{0II} + 2 \sum_{n=1}^{\infty} a_{nI} \cos(n(\pi - \phi)), \\
T_3 &= \sum_{-\infty}^{\infty} a_{nI} e^{-jn(\pi-\phi)} = -2i \sum_{n=1}^{\infty} a_{nI} \sin(n(\pi - \phi)), \\
T_4 &= \sum_{n=1}^{\infty} b_{nII} e^{-jn(\pi-\phi)} = -2i \sum_{n=1}^{\infty} b_{nII} \sin(n(\pi - \phi)) = -T_3, \\
\phi &= \phi_r - \phi_i, \\
a_{nI} &= \frac{C_n V_n - B_n D_n}{W_n V_n + j D_n^2}, \quad b_{nI} = \frac{W_n B_n + j D_n C_n}{W_n V_n + j D_n^2}, \\
a_{nII} &= -\frac{A_n V_n - j C_n D_n}{W_n V_n + j D_n^2}, \quad b_{nII} = -j \frac{C_n W_n + A_n D_n}{W_n V_n + j D_n^2}, \\
A_n &= j\xi [\xi J'_n(\gamma) J_n(\xi) - \gamma J_n(\gamma) J'_n(\xi)], \\
B_n &= \xi [\eta^2 \xi J'_n(\gamma) J_n(\xi) - \gamma J_n(\gamma) J'_n(\xi)], \\
C_n &= n \sin \theta_i \gamma J_n(\gamma) J_n(\xi) \left(\frac{\xi^2}{\gamma^2} - 1 \right), \\
D_n &= n \sin \theta_i \gamma J_n(\gamma) H_n^{(1)}(\xi) \left(\frac{\xi^2}{\gamma^2} - 1 \right), \\
V_n &= \xi \left[\eta^2 \xi J'_n(\gamma) H_n^{(1)}(\xi) - \gamma J_n(\gamma) H_n^{(1)'}(\xi) \right], \\
W_n &= j\xi \left[\gamma J_n(\gamma) H_n^{(1)'}(\xi) - \xi J'_n(\gamma) H_n^{(1)}(\xi) \right].
\end{aligned} \tag{56}$$

In above equations, parameters $\xi = ka \cos \theta_i$, $\gamma = ka \sqrt{\eta^2 - \sin^2 \theta_i}$ and a is the cylinder radius. J_n is the n th order Bessel function of the first kind. $H_n^{(1)}$ is the n th order Hankel function of the first kind. J'_n and $H_n^{(1)'}$ are the derivatives of J_n and $H_n^{(1)}$ respectively. In theory we need infinite number of terms ($n \rightarrow \infty$) in the expansion. However in practice, we can compute the desired number of terms that can achieve machine precision [16].

In the far field, the scattered intensity per unit length can be calculated as

$$I_s(\theta_i, \phi_i, \phi_r, \lambda) = \frac{|T_1|^2 + |T_2|^2 + |T_3|^2 + |T_4|^2}{\pi k}. \tag{57}$$

and the azimuthal function is

$$N_{\text{wave}}(\theta_i, \phi_i, \phi_r, \lambda) = \frac{I_s(\theta_i, \phi_i, \phi_r, \lambda)}{|W_x(\theta_i, \phi_i, \lambda)|} = \frac{|T_1|^2 + |T_2|^2 + |T_3|^2 + |T_4|^2}{2a\pi k \cos \theta_i}. \tag{58}$$

For more details of the Mie theory, we refer the readers to [2].

4 Gaussian beam

A Gaussian beam is a specific kind of electromagnetic wave with its amplitude being a Gaussian function in the transverse plane (the plane perpendicular to the propagating direction). In optics, a Gaussian beam is often used to model a laser beam. In our work, we validated the integration of our wave optics azimuthal function into the renderer by comparing the net effect of the fiber on the far-field radiance distribution. In the wave case, we used a 2.5D non-paraxial Gaussian beam to compute the net effect. The net effect is the total intensity minus the incident intensity. Unlike a plane wave, a Gaussian beam is a non-singular incident distribution, so we can take a meaningful far-field limit and compute the total field intensity minus incident field intensity. In addition, a Gaussian beam does not introduce actual simulation cost to our computation. One can post-process plane wave simulation results to produce beam solutions for any beam widths and offset values.

4.1 2.5D Gaussian beam

A non-paraxial 2.5D Gaussian beam satisfies Maxwell's equations. For simplicity, we first define a 2.5D Gaussian beam that satisfies the scalar wave equation. The vector form can be derived from the scalar form and the details are in Appendix A. We adopt the coordinate system shown in Figure 1 (a), and represent the 3D and 2D coordinates using $\mathbf{r} = x\hat{\mathbf{x}} + y\hat{\mathbf{y}} + z\hat{\mathbf{z}}$ and $\boldsymbol{\rho} = x\hat{\mathbf{x}} + y\hat{\mathbf{y}}$. Assume a Gaussian beam with waist w , centered at y_c with incident azimuthal direction $\phi_i = 0$. The $\phi_i \neq 0$ cases can be easily obtained via rotation. As in the previous section, $\mathbf{k} = \mathbf{k}_\rho + k_z\hat{\mathbf{z}}$ denotes the direction that is opposite to the wave propagation direction. At $x = 0$, the scalar field in the $y - z$ plane is defined as:

$$U(0, y, z) = e^{jk_z z} e^{-\frac{(y-y_c)^2}{w^2}}, \quad (59)$$

which for any specific z value ψ is a 1D Gaussian function. Define

$$g(y) = e^{-\frac{(y-y_c)^2}{w^2}}. \quad (60)$$

We denote the Fourier transform of a function g as either \tilde{g} or $\mathcal{F}[g]$ and denote the inverse Fourier transform as \mathcal{F}^{-1} . Equation (59) can also be written as

$$\begin{aligned} U(0, y, z) &= e^{jk_z z} \mathcal{F}^{-1}[\mathcal{F}[g(y)]] \\ &= e^{jk_z z} \mathcal{F}^{-1}[\tilde{g}(k_y)] \\ &= e^{jk_z z} \int_{-\infty}^{\infty} \tilde{g}(k_y) e^{-jk_y y} dk_y, \end{aligned} \quad (61)$$

where

$$\begin{aligned} \tilde{g}(k_y) &= \frac{1}{2\pi} \int_{-\infty}^{\infty} e^{-\frac{(y-y_c)^2}{w^2}} e^{jk_y y} dy \\ &= \frac{we^{-k_y^2 w^2/4} e^{jk_y y_c}}{2\sqrt{\pi}}. \end{aligned} \quad (62)$$

The full expression of the scalar Gaussian beam that satisfies the scalar wave equation can be written as

$$\begin{aligned} U(x, y, z) &= e^{jk_z z} \int_{-\infty}^{\infty} \tilde{g}(k_y) e^{-jk_x x} e^{-jk_y y} dk_y \\ &= e^{jk_z z} \int_{-\infty}^{\infty} \frac{w e^{-k_y^2 w^2/4} e^{jk_y y_c}}{2\sqrt{\pi}} e^{-jk_x x} e^{-jk_y y} dk_y, \end{aligned} \quad (63)$$

where $k_s^2 + k_y^2 = k_\rho^2$. We introduce $\phi_p = \arctan(\frac{k_y}{k_x}) = \arctan(\frac{k_y}{\sqrt{k_\rho^2 - k_y^2}})$. Then

$$d\phi_p = \frac{d}{dk_y} \left(\arctan\left(\frac{k_y}{\sqrt{k_\rho^2 - k_y^2}}\right) \right) dk_y = \frac{dk_y}{\sqrt{k_\rho^2 - k_y^2}} = \frac{dk_y}{k_x}. \quad (64)$$

Apply change of variable to Equation (63) and we get

$$\begin{aligned} U(x, y, z) &= e^{jk_z z} \int_{-\pi/2}^{\pi/2} \frac{w e^{-k_y^2 w^2/4} e^{jk_y y_c}}{2\sqrt{\pi}} e^{-jk_x x} e^{-jk_y y} k_x d\phi_p \\ &= e^{jk_z z} \int_{-\pi/2}^{\pi/2} \frac{w e^{-k_\rho^2 (\sin^2 \phi_p) w^2/4} e^{jk_\rho \sin \phi_p y_c}}{2\sqrt{\pi}} e^{-jk_\rho (x \cos \phi_p + y \sin \phi_p)} k_\rho \cos \phi_p d\phi_p \\ &= e^{jk_z z} \frac{k_\rho w}{2\sqrt{\pi}} \int_{-\pi/2}^{\pi/2} e^{-k_\rho^2 (\sin^2 \phi_p) w^2/4} e^{jk_\rho \sin \phi_p y_c} e^{-jk_\rho (x \cos \phi_p + y \sin \phi_p)} \cos \phi_p d\phi_p \\ &= e^{jk_z z} \frac{k_\rho w}{2\sqrt{\pi}} \int_{-\pi/2}^{\pi/2} \left(e^{-k_\rho^2 (\sin^2 \phi_p) w^2/4} e^{jk_\rho \sin \phi_p y_c} \cos \phi_p \right) e^{-jk_\rho (x \cos \phi_p + y \sin \phi_p)} d\phi_p \end{aligned} \quad (65)$$

In the above equation $e^{-jk_\rho (x \cos \phi_p + y \sin \phi_p)}$ is a scalar component of a plane wave. Equation (65) shows that the beam field can be expanded into a summation of an infinite number of plane waves (with different incident directions). This is the so-called Angular Spectrum Method [7] and we will show in the following how to use fast fourier transform (FFT) to compute the beam incidence solution from a plane wave incidence solution.

4.2 From plane wave incidence to Gaussian beam incidence

Consider a fiber of arbitrary cross section contained in a circumscribing circle of radius a . Upon illumination by the incident field

$$E_i^n(\boldsymbol{\rho}) = J_n(k\rho) e^{jn\phi}, \quad (66)$$

where $\boldsymbol{\rho} = x\hat{\mathbf{x}} + y\hat{\mathbf{y}}$, $\rho = |\boldsymbol{\rho}|$ and ϕ is the angle between $\boldsymbol{\rho}$ and the x -axis. The fiber scatters field $E_s(\boldsymbol{\rho})$ which for $\rho > a$ can be expressed in terms of outward propagating Hankel functions [8]

$$E_s^n(\boldsymbol{\rho}) = \sum_{m=N}^N b_{mn} H_m(k\rho) e^{jm\phi} \quad (67)$$

The scattered field is angularly band-limited and N is the required mode number. There exist many ways of computing the b_{mn} s. One could illuminate the scatterer with the incident fields $J_n(\rho)e^{jn\phi}$ (as opposed to the traditional plane wave) and compute the projection of the scattered field onto each outgoing harmonic $H_m(k\rho)e^{jm\phi}$ (as opposed to the traditional far field pattern). Alternatively, the b_{mn} s can be computed by post-processing the results obtained using a code that uses traditional plane wave excitations and computes far-field patterns.

Assume the fiber is excited by a plane wave coming from direction $\phi_p = 2\pi(p-1)/(2N+1)$ (uniformly spaced angles) given by

$$E_{i,\phi_p}(\boldsymbol{\rho}) = e^{j\mathbf{k}(\phi_p)\cdot\boldsymbol{\rho}} = \sum_{n=-N}^N j^n J_n(k\rho)e^{jn(\phi-\phi_p)} = \sum_{n=-N}^N j^n e^{-jn\phi_p} J_n(k\rho)e^{jn\phi} \quad (68)$$

By linearity, it follows from Equation (67) that for $\rho > a$, this scattered field can be expressed as

$$E_{s,\phi_p}(\boldsymbol{\rho}) = \sum_{n=-N}^N j^n e^{-jn\phi_p} \sum_{m=-N}^N b_{mn} H_m(k\rho) e^{jm\phi} \quad (69)$$

Using the large argument approximation of the Hankel function, this same field (for $\rho \gg a$) is given by

$$\begin{aligned} E_{s,\phi_p}(\boldsymbol{\rho}) &= \sum_{n=-N}^N j^n e^{-jn\phi_p} \sum_{m=-N}^N b_{mn} \sqrt{\frac{2j}{\pi k\rho}} j^m e^{-jk\rho} e^{jm\phi} \\ &= \frac{e^{-jk\rho}}{\sqrt{\rho}} \left(\sum_{m=-N}^N \sum_{n=-N}^N j^n e^{-jn\phi_p} b_{mn} \sqrt{\frac{2j}{\pi k\rho}} j^m e^{-jk\rho} e^{jm\phi} \right) \\ &= \frac{e^{-jk\rho}}{\sqrt{\rho}} \sum_{m=-N}^N \sum_{n=-N}^N \left(j^n b_{mn} \sqrt{\frac{2j}{\pi k}} j^m e^{-jk\rho} \right) e^{jm\phi} e^{-jn\phi_p} \\ &= \frac{e^{-jk\rho}}{\sqrt{\rho}} \sum_{m=-N}^N \sum_{n=-N}^N c_{mn} e^{jm\phi} e^{-jn\phi_p} \end{aligned} \quad (70)$$

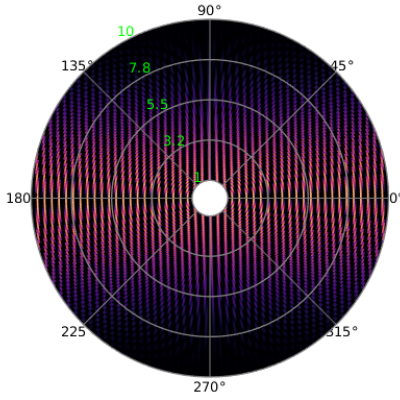
The last step is to relate the Gaussian beam expression Equation (65) and Equation (66) by expanding the plane wave component in Equation (65) using Equation (68). Then

Equation (65) becomes

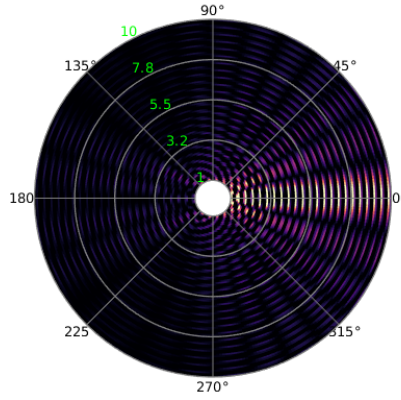
$$\begin{aligned}
U(x, y, z) &= e^{jk_z z} \frac{k_\rho w}{2\sqrt{\pi}} \int_{-\pi/2}^{\pi/2} \left(e^{-k_\rho^2 (\sin^2 \phi_p) w^2 / 4} e^{jk_\rho \sin \phi_p y_c \cos \phi_p} \right) e^{-jk_\rho (x \cos \phi_p + y \sin \phi_p)} d\phi_p \\
&= e^{jk_z z} \frac{k_\rho w}{2\sqrt{\pi}} \int_{-\pi/2}^{\pi/2} \left(e^{-k_\rho^2 (\sin^2 \phi_p) w^2 / 4} e^{jk_\rho \sin \phi_p y_c \cos \phi_p} \right) \sum_{n=-N}^N j^{-n} J_n(k_\rho \rho) e^{jn(\phi - \phi_p)} d\phi_p \\
&= e^{jk_z z} \frac{k_\rho w}{2\sqrt{\pi}} \sum_{n=-N}^N j^{-n} \left(\int_{-\pi/2}^{\pi/2} e^{-k_\rho^2 (\sin^2 \phi_p) w^2 / 4} e^{jk_\rho \sin \phi_p y_c} e^{-jn\phi_p} \cos \phi_p d\phi_p \right) J_n(k_\rho \rho) e^{jn\phi} \\
&= \sum_{n=-N}^N a_n J_n(k_\rho \rho) e^{jn\phi},
\end{aligned} \tag{71}$$

where we write the Gaussian beam in terms of expansion of the Bessel function where a_n s are the expansion coefficients. To compute the Gaussian beam incidence solution, we first conduct 2D inverse FFT computation on the plane wave incidence solutions to get c_{mn} s. Then from c_{mn} s we can compute b_{mn} s based on Equation (70). Finally we weight b_{mn} s by a_n s and conduct FFT to compute the Gaussian beam solution.

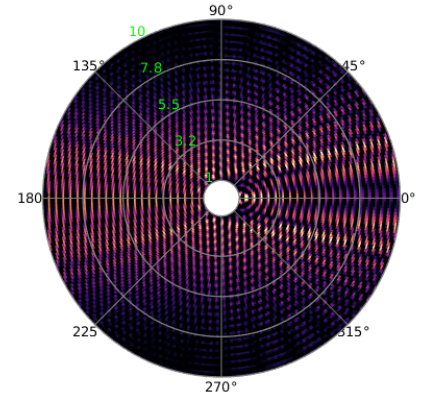
In the figure on the next page, we draw fields for Gaussian beam illuminating circular cross sections.



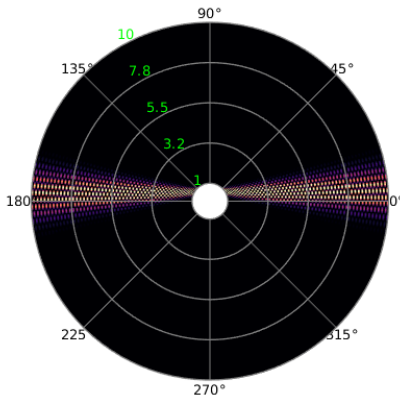
(a) $\text{Re}(\mathbf{E}_i)$, z component



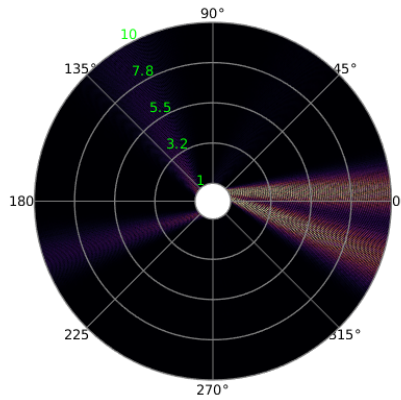
(b) $\text{Re}(\mathbf{E}_s)$, z component



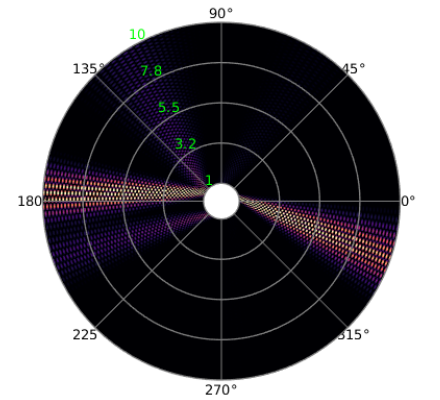
(c) $\text{Re}(\mathbf{E}_t)$, z component



(d) $\text{Re}(\mathbf{E}_i)$, z component



(e) $\text{Re}(\mathbf{E}_s)$, z component



(f) $\text{Re}(\mathbf{E}_t)$, z component

Figure 4: In this figure, we plot the fields for Gaussian beams illuminating circular cross sections. In the first row, we have a circle with radius $1\mu m$ and a Gaussian beam with waist $5\mu m$. In the second row, we have a circle with radius $10\mu m$ and Gaussian beam with waist $1\mu m$ and a center offset $5\mu m$. In both cases, Gaussian beams have wavelength $400nm$ and TM polarization. They are normally incident on the circular cross sections. We plot the real part of the z component of the electric fields. Non-positive values are shown as black. The first column is the incident field, the second column is the scattered field, and the third column is the total field. When the beam is wide (first row) it can be used to approximated plane wave incidence. When the beam is narrow (second row), the scattering pattern is similar to what we usually observe in ray optics despite the field oscillation and beam divergence.

References

- [1] Milton Abramowitz and Irene A Stegun. *Handbook of mathematical functions with formulas, graphs, and mathematical tables*, volume 55. US Government printing office, 1948. [3.2.6](#)
- [2] Craig F Bohren and Donald R Huffman. *Absorption and scattering of light by small particles*. John Wiley & Sons, 2008. ([document](#)), [3.3](#), [3.3](#)
- [3] Max Born and Emil Wolf. Principles of optics, chapter 1, 1999. ([document](#))
- [4] Weng Cho CHEW. Lectures on electromagnetic field theory, 2020. <https://engineering.purdue.edu/wcchew/ece604f20/EMFTAll.pdf>. ([document](#)), [2](#)
- [5] Eugene d’Eon, Guillaume Francois, Martin Hill, Joe Letteri, and Jean-Marie Aubry. An energy-conserving hair reflectance model. In *Proceedings of the Twenty-second Eurographics Conference on Rendering*, EGSR ’11, pages 1181–1187, Aire-la-Ville, Switzerland, Switzerland, 2011. Eurographics Association. [3](#)
- [6] Walton C Gibson. *The method of moments in electromagnetics*. Chapman and Hall/CRC, 2014. ([document](#)), [3.2.5](#)
- [7] Joseph W Goodman. *Introduction to Fourier optics*. Roberts and Company Publishers, 2005. [4.1](#)
- [8] RF Harrington and Time-Harmonic Electromagnetic Fields. pp. 460-463, 1961. ([document](#)), [2](#), [2.1](#), [2.1](#), [4.2](#), [A](#)
- [9] John David Jackson. Classical electrodynamics, 1999. ([document](#)), [2](#), [2.3](#), [3.1](#), [3.2.1](#)
- [10] Augustus Edward Hough Love. I. the integration of the equations of propagation of electric waves. *Philosophical Transactions of the Royal Society of London. Series A, Containing Papers of a Mathematical or Physical Character*, 197(287-299):1–45, 1901. [3.2](#), [3.2.1](#)
- [11] Andrew J Poggio and Edmund K Miller. *Integral equation solutions of three-dimensional scattering problems*. MB Assoc., 1970. [3.2.4](#)
- [12] Thomas Rylander, Pär Ingelström, and Anders Bondeson. *Computational electromagnetics*. Springer Science & Business Media, 2012. [3.2.2](#), [3.2.5](#)
- [13] SA Schelkunoff. Some equivalence theorems of electromagnetics and their application to radiation problems. *The Bell System Technical Journal*, 15(1):92–112, 1936. [3.2](#), [3.2.1](#)
- [14] Steven H Schot. Eighty years of sommerfeld’s radiation condition. *Historia mathematica*, 19(4):385–401, 1992. [3.2.2](#)
- [15] Allen Taflove and Susan C Hagness. *Computational electrodynamics: the finite-difference time-domain method*. Artech house, 2005. ([document](#))

- [16] Warren J Wiscombe. Improved mie scattering algorithms. *Applied optics*, 19(9):1505–1509, 1980. [3.3](#)

A Vector fields derivation

We can construct a vector field representation from a scalar field. Assume ψ satisfies the scalar wave equation $\nabla^2\psi + k^2\psi = 0$. For TM polarization, we construct the electric field and magnetic field components as [8]:

$$\begin{aligned} E_x &= \frac{1}{\hat{y}} \frac{\partial^2 \psi}{\partial x \partial z}, E_y = \frac{1}{\hat{y}} \frac{\partial^2 \psi}{\partial y \partial z}, E_z = \frac{1}{\hat{y}} \left(\frac{\partial^2}{\partial z^2} + k^2 \right) \psi, \\ H_x &= \frac{\partial \psi}{\partial y}, H_y = -\frac{\partial \psi}{\partial x}, H_z = 0, \\ \hat{y} &= j\omega\epsilon. \end{aligned}$$

So

$$\begin{aligned} E_x &= \frac{1}{j\omega\epsilon} (jk_x)(jk_z)\psi = -\frac{k_x k_z}{j\omega\epsilon} \psi, \\ E_y &= \frac{1}{j\omega\epsilon} (jk_y)(jk_z)\psi = -\frac{k_y k_z}{j\omega\epsilon} \psi, \\ E_z &= \frac{1}{j\omega\epsilon} (k^2 - k_z^2)\psi = \frac{k_\rho^2}{j\omega\epsilon} \psi, \\ H_x &= jk_y \psi, \\ H_y &= -jk_x \psi, \\ H_z &= 0. \end{aligned}$$

If we let E_z be the scalar Fourier component U in Equation (65), then we have

$$\begin{aligned} \psi &= \frac{E_z j\omega\epsilon}{k_\rho^2} = \frac{U j\omega\epsilon}{k_\rho^2} \\ E_x &= -\frac{k_x k_z}{j\omega\epsilon} \frac{U j\omega\epsilon}{k_\rho^2} = \frac{-\sin\theta \cos\phi U}{\cos\theta} \\ E_y &= -\frac{k_y k_z}{j\omega\epsilon} \frac{U j\omega\epsilon}{k_\rho^2} = \frac{-\sin\theta \sin\phi U}{\cos\theta} \\ H_x &= -\frac{\sin\phi U \omega\epsilon}{k \cos\theta} \\ H_y &= \frac{\cos\phi U \omega\epsilon}{k \cos\theta} \\ H_z &= 0 \end{aligned}$$

For TE polarization, we construct the electric field and magnetic field components as [8]:

$$\begin{aligned}
E_x &= -\frac{\partial\psi}{\partial y}, E_y = \frac{\partial\psi}{\partial x}, E_z = 0, \\
H_x &= \frac{1}{\hat{z}} \frac{\partial^2\psi}{\partial x\partial z}, H_y = \frac{1}{\hat{z}} \frac{\partial^2\psi}{\partial y\partial z}, H_z = \frac{1}{\hat{z}} \left(\frac{\partial^2}{\partial z^2} + k^2 \right) \psi \\
\hat{z} &= j\omega\mu
\end{aligned}$$

If we let H_z be the scalar Fourier component U in Equation (65), then we have

$$\begin{aligned}
\psi &= \frac{H_z j\omega\mu}{k_\rho^2} = \frac{U j\omega\mu}{k_\rho^2} \\
E_x &= \frac{\sin\phi U \omega\mu}{k \cos\theta} \\
E_y &= -\frac{\cos\phi U \omega\mu}{k \cos\theta} \\
E_z &= 0 \\
H_x &= -\frac{k_x k_z U j\omega\epsilon}{j\omega\epsilon k_\rho^2} = \frac{-\sin\theta \cos\phi U}{\cos\theta} \\
H_y &= -\frac{k_y k_z U j\omega\epsilon}{j\omega\epsilon k_\rho^2} = \frac{-\sin\theta \sin\phi U}{\cos\theta}
\end{aligned} \tag{72}$$